Dependence of stacking-fault nucleation on cluster mobility

Celia Polop,* Andreas Lammerschop, Carsten Busse,† and Thomas Michely
I. Physikalisches Institut, RWTH Aachen, 52056 Aachen, Germany
(Received 3 October 2004; published 25 March 2005)

A set of rate equations is presented that allows one to predict stacking-fault probabilities and island number densities in homoepitaxial growth. This set is shown to accurately reproduce the available experiments for homoepitaxial growth on Ir(111). Moreover, based on an analysis of the atomistic data describing stacking and diffusion on fcc(111) surfaces, three model cases are studied. They yield surprising insights into the importance of cluster mobility for stacking-fault island formation.

DOI: 10.1103/PhysRevB.71.125423 PACS number(s): 68.55.Ac, 68.35.Dv, 68.35.Fx, 81.15.Aa

I. INTRODUCTION

The face-centered-cubic (fcc) and hexagonal-close-packed (hcp) crystal structures, as well as the homologous zinc-blende and wurtzite crystal structures with a two-atom base, differ only in the stacking sequence between successive dense-packed layers. The stacking sequence for the fcc and zinc-blende crystal structures is *ABCABC* in the [111] direction, whereas for hcp and wurtzite crystal structures it is *ABAB* in the [0001] direction. Errors in the stacking sequence—stacking faults—are frequently formed during textured or expitaxial thin-film growth and may strongly affect mechanical, electronic, optical, and magnetic properties of the film. Examples relate to the growth of GaN films,[1,2] epitaxial growth of ZnSe on GaAs(001),[3,4] Pt on Ni(111),[5] BN on Ni(111),[6] and Co on W(110)[7,8] and on Cu(111).[9,10] Even in homoepitaxy stacking faults are formed. Among the known systems are Si/Si(111),[11,12] Ag/Ag(111),[13–15] Cu/Cu(111),[16,17] and Ir/Ir(111).[18–20]

In a recent paper, we developed an atomistic model able to explain qualitatively the temperature dependence of stacking-fault formation in homoepitaxy on Ir(111).[18] At a given temperature the equilibrium (Boltzmann) distribution of the largest mobile cluster over regular and faulted sites determines the distribution of large stable islands in the two stackings: the largest mobile cluster will be immobilized by the addition of an adatom and remain in the initial stacking during subsequent growth.

Rate equations have been widely used to model nucleation and growth processes on surfaces. Initially rate equations were employed to describe nucleation on homogeneous surfaces with an uniform distribution of equivalent adsorption sites.[21,22] Successive modifications have spread out their application scope to more complex phenomena, such as nucleation and growth in the presence of island-edge barriers,[23] impurities,[24,25] nonlocal adatom-adatom interactions,[26,27] and surface reconstruction.[28,29] To solve the problem of stacking-fault nucleation we expanded the rate-equation approach to take the two inequivalent adsorption sites into account and reached quantitative agreement between measurements and experiments for the temperature dependence of stacking-fault formation.[18]

Here we present the full details of this approach (Sec. II) and demonstrate its power by comparison to the experimental results for temperature and flux dependence of the total island number densities as well as temperature and flux dependence of the stacking fault probability in homoepitaxial growth on Ir(111) (Sec. III). In Sec. IV we construct a fcc(111) model system allowing us to explore the roles of stacking-fault energy and cluster mobility in the kinetics of stacking-fault formation with the help of rate equations. The conclusions of this investigation are qualitatively confirmed by comparison to the known experimental data.

II. RATE EQUATIONS FOR STACKING-FAULT NUCLEATION

In this section we develop a formal description for nucleation in the presence of two inequivalent adsorption sites with the help of rate equations. Without loss of generality, we will consider here the fcc(111) surface with regular threefold coordinated adsorption sites (fcc sites *f*) and irregular threefold coordinated adsorption sites (hcp sites *h*). Adatoms move by passing alternatingly over *f* and *h* sites, implying jumps over two different kinetic barriers: $E^f_{\mathrm{d},1}$ for jumps starting from an *f* site and $E^h_{\mathrm{d},1}$ for jumps starting from an *h* site. The larger of the two activation energies $E^s_{\mathrm{d},1}$ (stacking type $s=f,h$) is linked with the lower one $E^{s'}_{d,1}$ ($s\neq s'$) by the binding energy difference of the adatom in the two adsorption sites $E^{s'}_{\mathrm{d},1}=E^s_{\mathrm{d},1}-|\Delta E_{\mathrm{b},1}|$.

Adatom clusters on the fcc(111) surface are built out of adatoms in sites separated by the in-plane lattice parameter a_{nn} such that each cluster has a specific stacking type *s*. Although the actual diffusion mechanisms of clusters on fcc(111) surfaces are complex,[30,31] we assume here clusters as rigid objects that move as a whole by jumps from one local minimum in the potential energy landscape to the next one, alternating between *f* and *h* stacking. For the problem under concern and cluster sizes up to heptamers this assumption is the simplest possible, reasonable assumption to approximate the rate of change between *f* and *h* sites and the global cluster motion.[32] As for adatoms, in this description the activation energies of jumps for a cluster of size *i* out of the two inequivalent sites are linked by $E^{s'}_{\mathrm{d,i}}=E^s_{d,i}-|\Delta E_{b,i}|$. According to transition state theory we thus define the jump rate of adatoms and clusters out of a specific stacking type *s* as

$$\nu_i^s = \nu_{0,i}^s e^{-E_{\mathrm{d},i}^s/k_\mathrm{B}T}, \tag{1}$$

where $\nu_{0,i}^s$ is the attempt frequency prefactor, T is the temperature, and k_B is the Boltzmann constant. Formally, we may link to these rates diffusion coefficients of adatoms and clusters in a specific stacking

$$D_i^s = \frac{\nu_{0,i}^s a_{fh}^2}{4} e^{-E_{\mathrm{d},i}^s/k_\mathrm{B}T}, \tag{2}$$

where $a_{fh}=a_{\mathrm{nn}}/\sqrt{3}$ is the jump width, i.e., the distance between two adjacent and inequivalent adsorption sites. The quantities ν_i^s and D_i^s, needed below for insertion into the rate equations, require the knowledge of $\nu_{0,i}^s$ and $E_{\mathrm{d},i}^s$, which are generally not accessible to experiment. How reasonable estimates of these quantities can be obtained will be outlined in the following sections (compare also Ref. 32).

Besides ν_i^s and D_i^s, the dissociation rates Γ_2^f and Γ_2^h for dimers in the respective stacking also enter the rate equations. We neglect dissociation of clusters larger than dimers, as on fcc(111) surfaces their dissociation becomes significant only at high temperatures. For these temperatures even on large terraces no more islands nucleate, i.e., no experimental data are available for comparison to the calculation. Other parameters in the rate equations are the capture numbers σ_i of clusters of size i, which are assumed to be equal for both types of stacking. We use the following capture numbers for all calculations: $\sigma_i=3$ for $i<8$ and $\sigma_i=\sigma_x=7$ for $i\geqslant 8$ as simple yet reasonable approximations.[22,33] Finally, the fractional coverage of the surface Θ and the deposition rate F enter, which are taken identical to the experiments to which the calculation is compared. Clusters with stacking s above a size $i\geqslant 8$ are considered immobile and counted together in n_x^s. This strong assumption limits the applicability of our model with respect to high temperatures, where clusters with $i\geqslant 8$ might be mobile. On the other hand, it keeps the number of rate equations and also the number of required experimental input parameters limited. All this leads to four expressions ($i=1, i=2, 2<i<8, i\geqslant 8$), which describe the time evolution of the density of i-size clusters with stacking s

$$\frac{dn_1^s}{dt} = \frac{F(1-\Theta)}{2} - \sigma_1 n_1^s D_1^{s'} n_1^{s'} - D_1^s n_1^s \sum_{j=1}^{7} \sigma_j n_j^{s'} - D_1^s n_1^s \sigma_x n_x^{s'} + \sum_{p=f,h} \Gamma_2^p n_2^p - n_1^s \nu_1^s + n_1^{s'} \nu_1^{s'}, \tag{3}$$

$$\frac{dn_2^s}{dt} = -\sigma_2 n_2^s \sum_{j=1}^{2} D_j^{s'} n_j^{s'} - D_2^s n_2^s \sum_{j=2}^{7} \sigma_j n_j^{s'} - D_2^s n_2^s \sigma_x n_x^{s'} + D_1^{s'} n_1^{s'} \sigma_1 n_1^s - \Gamma_2^s n_2^s - n_2^s \nu_2^s + n_2^{s'} \nu_2^{s'}, \tag{4}$$

$$\frac{dn_i^s}{dt} = -\sigma_i n_i^s \sum_{j=1}^{i} D_j^{s'} n_j^{s'} - D_i^s n_i^s \sum_{j=i}^{7} \sigma_j n_j^{s'} - D_i^s n_i^s \sigma_x n_x^{s'} + \sum_{j=1}^{i\mathrm{DIV2}} D_j^{s'} n_j^{s'} \sigma_{i-j} n_{i-j}^s - n_i^s \nu_i^s + n_i^{s'} \nu_i^{s'}, \tag{5}$$

$$\frac{dn_x^s}{dt} = \sum_{k=4}^{7} \sigma_k n_k^s \sum_{j=8-k}^{k} D_j^{s'} n_j^{s'}. \tag{6}$$

Equation (3) describes the time variation of monomers with stacking s. The terms on the right-hand side account for deposition with rate F, neglecting the adsorption on already occupied sites (the factor $\frac{1}{2}$ takes care of the two inequivalent adsorption sites); for s'-monomer attachment to s monomers ($s\neq s'$); for s-monomer attachment to monomers or to larger clusters of stacking type s' and size $i<8$ (note that only association between monomers or clusters with different stacking is feasible); for s-monomer attachment to s'-type clusters of size $i\geqslant 8$; for dimer dissociation creating two monomers (here we assume dimer dissociation of a cluster with stacking s to yield both an s and an s' monomer); and for jumps between the inequivalent binding sites. The most important extension of the rate equations is given by the last two terms, $n_1^s \nu_1^s$ and $n_1^{s'} \nu_1^{s'}$, which correspond to the loss and gain of adatoms of stacking s by jumps out of s and into s sites, respectively. Finally, we note that in our previous work,[18] a version of Eq. (3) with additional, incorrect terms was given. However, the quantitative results presented in Ref. 18 deviate only marginally from the correct calculations presented below.

The general equation for mobile and stable clusters is given by Eq. (5) in which the terms of the right-hand side describe the capture of smaller or equal-size s' clusters, the attachment of the cluster to an equal size s' cluster or to a larger one of size $i<8$, the attachment of the cluster to an s' cluster of size $i\geqslant 8$, the formation of clusters by aggregation of smaller ones that take over the stacking state of the capturer [here iDIV2$=i/2$ for i even and iDIV2$=(i-1)/2$ for i odd], and the jump of s-type (s'-type) clusters to s' sites (s sites).

Equation (4) for the time variation of the dimer density contains the same processes as specified above for Eq. (5), but has, in addition, the dimer dissociation term included.

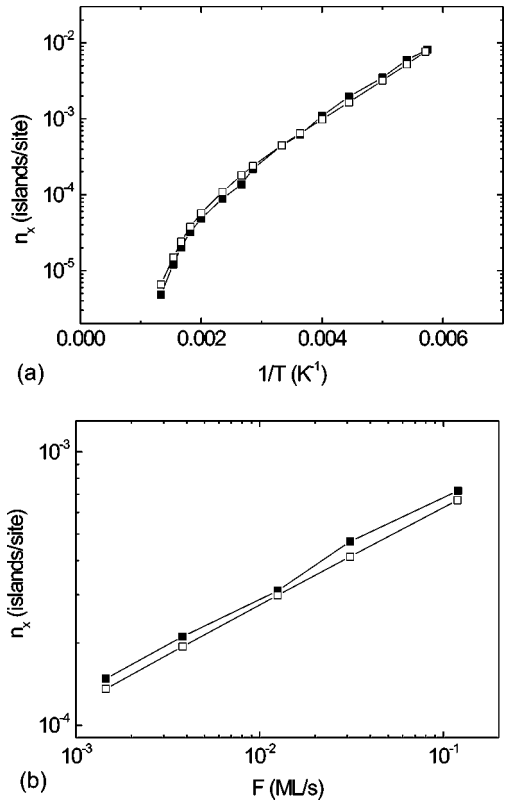

FIG. 1. (a) Temperature dependence ($F=0.013$ ML/s) and (b) rate dependence ($T=330$ K) of the total island density n_x in Ir(111). Black symbols correspond to the experimental data and open symbols to the solution of the rate equations.

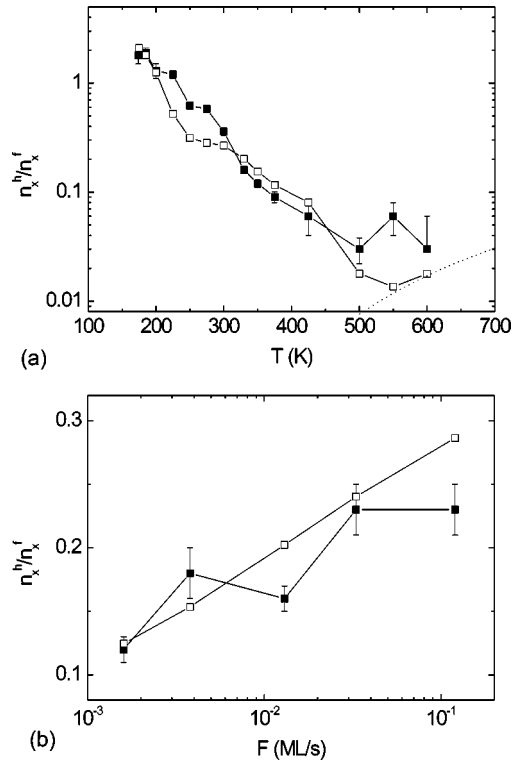

FIG. 2. (a) Temperature dependence ($F=0.013$ ML/s) and (b) rate dependence ($T=330$ K) of the stacking-fault probability in Ir(111). Black symbols correspond to the experimental data and open symbols to the solution of the rate equations. Dotted line corresponds to the Boltzmann distribution of the heptamers.

The time variation of immobile and stable clusters is given by Eq. (6), which takes into account all the association processes, resulting in clusters bigger than heptamers with stacking s.

III. APPLICATION TO HOMOEPITAXY ON Ir(111)

For homoepitaxial growth on Ir(111) the total adatom island density $n_x=n_x^f+n_x^h$ and the stacking-fault nucleation probability given by the ratio n_x^h/n_x^f were measured over a broad temperature and deposition rate range[18,34] as shown in Figs. 1 and 2 (full symbols). Here we demonstrate that these data may be reproduced very well by numerical integration of the 16 rate equations specified in Sec. II.

As a first requirement for the solution of the rate equations, the atomistic input data $\nu_{0,i}^s$, $E_{\mathrm{d},i}^s$, and Γ_2^s are needed. The adatom diffusion parameters $\nu_{0,1}^h$, $\nu_{0,1}^f$, $E_{\mathrm{d},1}^h$, and $E_{\mathrm{d},1}^f$ were directly measured by field ion microscopy.[35] From field ion microscopy also the global diffusion coefficients $D_i=D_{0,i}e^{E_{\mathrm{d},i}/k_{\mathrm{B}}T}$ for cluster sizes $2\leqslant i\leqslant 7$ are known.[30,31] In addition also the distribution of clusters over f and h sites was measured for cluster sizes $2\leqslant i\leqslant 4$ (Ref. 31), yielding the free energy difference ΔF_i between f and h sites. For cluster sizes $5\leqslant i\leqslant 7$ the binding energy difference $\Delta E_{\mathrm{b,i}}$ has been estimated.[18,32] From these measurements the desired data are obtained as follows: the larger of the two activation energies $E_{\mathrm{d,i}}^h$ and $E_{\mathrm{d,i}}^f$ is set identical to the effective, measured value $E_{\mathrm{d,i}}$; the smaller one is obtained by subtracting ΔF_i (or $\Delta E_{\mathrm{b,i}}$). The attempt frequency prefactors $\nu_{0,i}^h$ and $\nu_{0,i}^f$ are both set identical to an effective prefactor $\nu_{0,i}$ which is obtained by estimating $\nu_{0,i}=4D_{0,i}/a_{\mathrm{nn}}^2$. Finally, the experimental,[34] effective dissociation rate $\Gamma_2=\nu_{0,\mathrm{diss}}e^{E_{\mathrm{diss}}/k_{\mathrm{B}}T}$ is used as the dissociation rate of the easier process, whereas for the more difficult process the free energy difference ΔF_2 is added to E_{diss}. These approximations are less crude as they may appear at first sight and are discussed in detail in Ref. 32. The actual data used can be read from Table 1 of Ref. 18. Finally, for the solution of the rate equations, F and Θ were set to the experimental values.

Comparison of the calculations (open symbols) to the experimental data (full symbols) is made in Figs. 1 and 2. As can be seen in Fig. 1, the calculated total island number density n_x agrees very well with the measured one for all temperatures and fluxes. Figure 2(a) was already reproduced in Ref. 18 and shows the agreement of calculation and experiment for the ratio of faulted islands to regular islands in dependence of temperature. According to the construction of the rate equations, at high temperatures the calculated ratio between h and f islands must approach the Boltzmann distribution of the largest cluster being able to become mobile. In the present case the largest cluster becoming mobile is the heptamer. It is seen in Fig. 2(a) that the calculated values for n_x^h/n_x^f approach the Boltzmann distribution of the heptamer [dotted line in Fig. 2(a)] at 550 K. This temperature, thus, represents the high-temperature limit of validity for our cal-

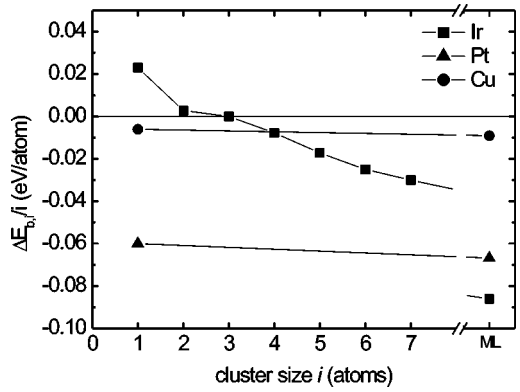

FIG. 3. Cluster size dependence of the difference in binding energy per atom $\Delta E_{b,i}/i$ for Ir,[18,31,35,39] Pt,[40] and Cu.[41] The values for a complete monolayer (ML) are the bulk-twin fault energies taken from Ref. 36 for Ir, from Ref. 42 for Pt, and from Ref. 43 for Cu (see text).

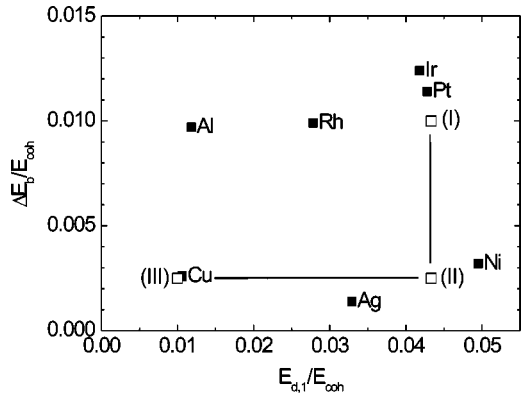

FIG. 4. Stacking-fault energy (Refs. 36, 42, 43, and 45) vs activation energy for monomer diffusion (Refs. 30, 41, and 46–52) for some selected fcc metals. Open squares denote the three studied cases.

culations. Finally, Fig. 2(b) exhibits the calculations for the flux dependence of the ratio of faulted island to regular islands at 330 K. While the calculations reproduce the experimental trend, the overall agreement is only moderate due to scatter of the experimental data. It should be noted that varying the deposition rate by two orders of magnitude only changes the probability of stacking-fault formation by less than a factor of three, whereas changing the temperature has a much more pronounced effect. Therefore, we will in the following concentrate on the temperature dependence of stacking-fault formation.

We have also performed additional calculations neglecting dimer dissociation. The results for the stacking-fault nucleation probability show only negligible changes. At the temperature of dimer dissociation even the largest mobile cluster considered in our calculations—the heptamer—is mobile. Thus, dimers dissociate only at such high temperatures, where the validity of our calculations for the prediction of the stacking-fault probability is anyway hampered by the artificial cutoff in the cluster mobility at $i=8$. Additionally we found that the terms in Eqs. (3)–(6), which largely determine the island densities for each type of cluster (f and h), are those related with the jump of clusters between the f and h sites and those where monomer diffusion is involved (i.e., association of monomers with other monomers or clusters). This is expected because, first, exchange of clusters between both stacking sites is a process needed to account for different stacking probabilities, and second, monomers have the largest diffusion coefficients and, consequently, these processes give rise to the largest rates. The rest of the terms can be neglected without significantly changing the accuracy of the model predictions.

IV. DEPENDENCE OF STACKING-FAULT NUCLEATION ON FAULT ENERGY AND CLUSTER MOBILITY

In this key section, the rate-equation approach developed in Sec. II will be used to explore the kinetics of stacking-fault formation. To this purpose an fcc(111) model system is constructed. The properties of the model system will be derived in a realistic manner from the current knowledge on binding energy differences between f and h sites and cluster mobilities for fcc(111) surfaces. The model system will be used as a vehicle to move, in a meaningful way, through the available parameter space. However, it does not represent any actual material.

In a first step we try to gain an understanding of how the binding energy differences $\Delta E_{b,i}$ typically depend on the cluster size i for fcc(111) surfaces. In Fig. 3 the cluster-binding energy difference per atom $\Delta E_{b,i}/i$ is plotted against the cluster size i (note also the axis break after $i=7$). The difference in binding energy per atom for a complete monolayer ΔE_b (or stacking-fault energy) was assumed to be equal to the bulk twin-fault energy (if available the experimental value for this quantity was used). We note that a surface stacking fault presents a situation closer to a bulk twin fault than to an intrinsic or extrinsic stacking fault that consists of two correlated stacking faults. Consequently, we expect that the twin-fault energy approaches better to the difference in binding energy per atom for a complete monolayer, as it was obtained for Ir(111) in support of our assumption.[19,36] For the case of Ir, the difference in binding energy per atom $\Delta E_{b,i}/i$ depends strongly on the cluster size and even changes the sign. Adatoms strongly prefer h sites, trimer atoms are found with equal probability on h and f sites, and atoms in larger clusters energetically prefer the regular f sites more and more. As pointed out by Papadia *et al.*[37] with increasing d-electron filling for transition metals, a change from hcp to fcc stacking occurs. For elements having a d-electron filling just sufficient to establish fcc stacking in the bulk, adatoms and small clusters experiencing a smaller effective d-electron density than the bulk still prefer the h sites. Though Ir is the only case where this behavior has been measured experimentally,[31] recent *ab initio* calculations indicate the same behavior for Rh,[38] which is also located at the boundary between hcp and fcc stacking. For elements with d-electron filling well above the hcp-fcc boundary a different behavior seems to be more typical. As suggested by the cases of Pt and Cu in Fig. 3, for these elements the difference in binding energy per atom appears to be largely independent from the cluster size and close to the stacking-fault energy

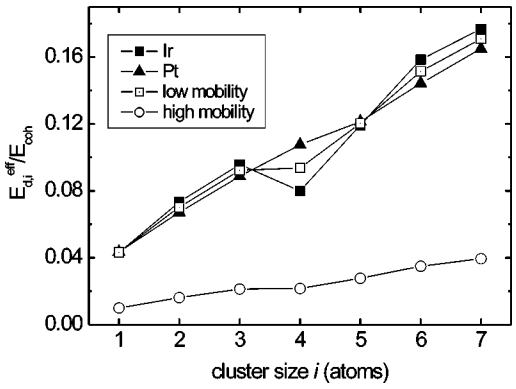

FIG. 5. Normalized effective activation energies $E_{d,i}^{\mathrm{eff}}/E_{\mathrm{coh}}$ of cluster diffusion for Ir(111) and Pt(111) and for the low-mobility (I and II) and high-mobility (III) model cases (see text).

ΔE_{b}. For the model system, we will consider this simpler and probably more frequent case and assume $\Delta E_{\mathrm{b},i}=i\Delta E_{\mathrm{b}}$.

In a second step we need to obtain an overview on the parameter space of stacking-fault energies versus cluster mobilities. In order to make the available data for the different materials comparable, they need to be normalized to the respective cohesive energies E_{coh}.[44] For the cluster mobilities we choose, for lack of better knowledge, the activation energy of adatom diffusion $E_{\mathrm{d},1}$ as an indicator (see also below): a low (high) scaled activation energy of adatom diffusion is assumed to indicate low (high) activation energies of cluster diffusion. As above for the stacking-fault energy ΔE_{b}, we use the twin-fault energy (again, if available, the experimental value). Figure 4 gives a survey of $\Delta E_{\mathrm{b}}/E_{\mathrm{coh}}$ versus $E_{\mathrm{d},1}/E_{\mathrm{coh}}$ for selected fcc(111) surfaces. Based on this data representation one may distinguish two groups of metals with low (Cu, Ag, Ni) and high (Al, Rh, Ir, Pt) stacking-fault energy, while the mobility decreases from Cu at the high-mobility side to Ni at the low-mobility side. To explore this parameter space we choose for the model system three different situations denoted by I, II, and III in Fig. 4: Case I represents large stacking-fault energy and low mobility ($\Delta E_{\mathrm{b}}/E_{\mathrm{coh}}=0.01$ and $E_{\mathrm{d},1}/E_{\mathrm{coh}}=0.043$); case II, small stacking-fault energy and low mobility ($\Delta E_{\mathrm{b}}/E_{\mathrm{coh}}=0.0025$ and $E_{\mathrm{d},1}/E_{\mathrm{coh}}=0.043$); and finally case III, small stacking-fault energy and high mobility ($\Delta E_{\mathrm{b}}/E_{\mathrm{coh}}=0.0025$ and $E_{\mathrm{d},1}/E_{\mathrm{coh}}=0.01$). By varying independently both parameters, their influence on the stacking-fault nucleation can be studied.

Before starting to solve the rate equations for the three cases (I, II, and III) constructed above, in a third step we need to specify explicitly the cluster mobilities. The global cluster diffusion coefficients, activation energies, and attempt frequency prefactors were measured experimentally only for Ir(111) and Pt(111).[30,31,53] In order to make the activation energies comparable we work with a single, generalized attempt frequency $\nu_0=5\times10^{12}\ \mathrm{s}^{-1}$. This value for ν_0 is around the average of the measured cluster diffusion attempt frequencies[30,31,53] and matches in the temperature range of interest the universal prefactor $k_{\mathrm{B}}T/h$ of transition state theory. We calculated effective activation energies $E_{\mathrm{d,i}}^{\mathrm{eff}}$ by defining $E_{\mathrm{d,i}}^{\mathrm{eff}}=k_{\mathrm{B}}T_{1,i}\ln\nu_0$ for both systems. Here, $T_{1,i}$ is the

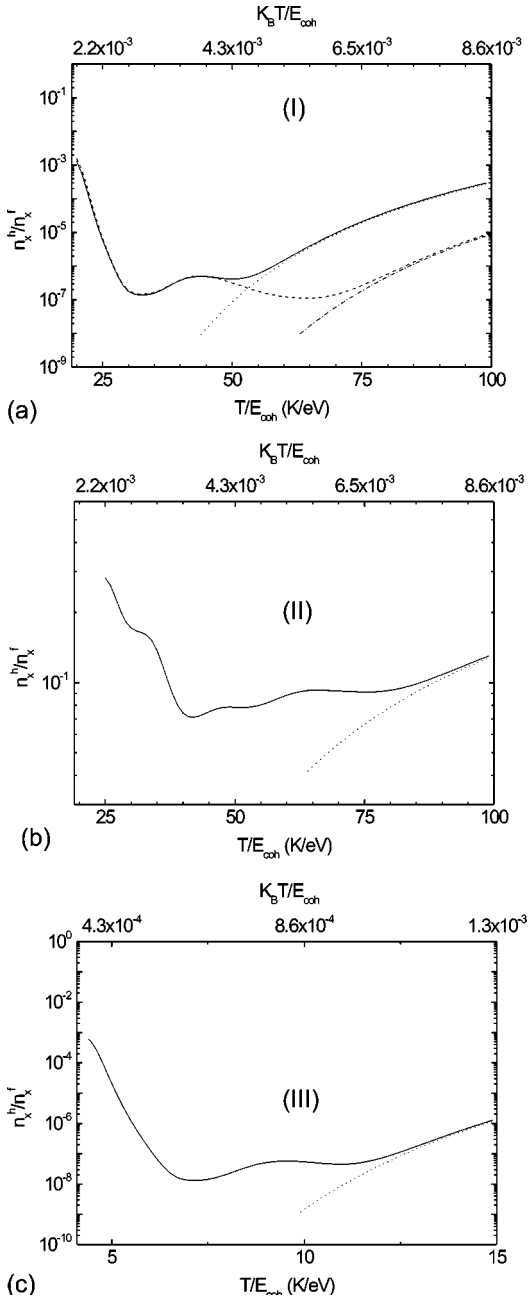

FIG. 6. Temperature dependence of the stacking-fault probability for the three model cases (I, II, and III). Full line: solution of rate equations with the heptamer being the largest cluster becoming mobile. Dotted line: Boltzmann distribution of the heptamer. Dashed line: solution of rate equations with the 10-atom cluster being the largest cluster becoming mobile. Dash-dotted line: Boltzmann distribution of the 10-atom cluster.

temperature at which the i cluster has a jump rate $\nu_i=1\ \mathrm{s}^{-1}$, and $T_{1,i}$ is calculated from the measured values of $E_{\mathrm{d,i}}$ and $\nu_{0,i}$. Note that at $T_{1,i}$, where the mobility of the cluster becomes relevant, the jump rates ν_i and ν_i^{eff} calculated with the measured and effective values coincide. The effective activation energies $E_{\mathrm{d,i}}^{\mathrm{eff}}$ for Ir and Pt are represented in Fig. 5 (black symbols). Both materials show the same trend, so we use the average of both data sets as effective activation energies $E_{\mathrm{d,i}}^{\mathrm{eff}}$ for the low-mobility cases I and II (open squares in Fig. 5).

TABLE I. Results for different materials: Normalized stacking-fault energy $\Delta E_b/E_{coh}$, normalized activation energy for adatom diffusion $E_{d,1}/E_{coh}$; temperature T_{exp} at which the stacking-fault probability P_{exp} has been experimentally measured; and temperature T_{RE} at which the stacking-fault probability P_{RE} is calculated by the rate-equation approach.

	$\Delta E_b/E_{coh}$	$E_{d,1}/E_{coh}$	T_{exp} (K)	P_{exp}	T_{RE} (K)	P_{RE}
Pt	0.0114	0.0435	>150	no SF[a]	169	$\approx 10^{-7}$
Ag	0.0024	0.0329	120	0.04[b]	120	0.16
			220	0.25[c]	220	0.16
Cu	0.0023	0.0106	286	no SF on flat surface[d]	40	$\approx 10^{-8}$
			215–400	0.2–0.7 on stepped surface[e]		
Al	0.0097	0.0118	>68	no SF[a]		

[a]Reference 55.
[b]Reference 54.
[c]Reference 14.
[d]Reference 17.
[e]Reference 16.

The effective activation energies for the high-mobility case III are obtained by scaling down the previous activation energies by a factor of 4.3, such that the condition $E_{d,1}^{eff}/E_{coh} = 0.01$ is fulfilled (open circles in Fig. 5). From these two sets of diffusion barriers $E_{d,i}^{eff}$, we compute the diffusion barrier for every adsorption site in the model system as $E_{d,i}^{eff,f} = E_{d,i}^{eff}$ and $E_{d,i}^{eff,h} = E_{d,i}^{eff} - i\Delta E_b$. Finally, we neglect dimer dissociation in the model system. Now we are ready to numerically integrate the set of 16 equations for the three selected situations.

Figures 6(a)–6(c) display the results of our calculations for the three cases (I, II, and III). In each figure the full line represents the stacking-fault probability n_x^h/n_x^f and the dotted line, the Boltzmann distribution for the heptamer. Despite the different scales of x and y axes, the three stacking-fault probability curves exhibit a similar shape characterized by three ranges. At low temperatures the stacking-fault probability decreases rapidly, stays on a base level at intermediate temperatures, and eventually approaches the Boltzmann distribution of the heptamers at high temperatures. To get a deeper physical insight into the results, we recall[18] that at a given temperature T the stacking-fault probability P is roughly given by

$$P = \frac{n_x^h}{n_x^f} \approx e^{-(i^\dagger \Delta E_b/k_B T)}, \tag{7}$$

where $i^\dagger$ denotes the size of the largest mobile cluster at this temperature. Although $i^\dagger$ strictly represents natural numbers, in this oversimplified treatment it may be considered as a continuous function determined by some effective diffusivity of the relevant mobile clusters. The particular shape of the stacking-fault probability curves depends on the specific diffusion barriers we chose in each case. The common feature to all cases is that, due to the limitation of the number of cluster diffusion coefficients taken into account, the heptamer stays the largest mobile cluster beyond a critical cutoff temperature T_c. Thus for $T > T_c$ our calculated stacking-fault ratio approaches to the Boltzmann distribution of the heptamer. T_c, thus, defines the limit of validity of our calculations. We also tested the effect of taking into account an increased number of clusters. By linear extrapolation of the activation energies from $E_{d,4}^{eff}$ to $E_{d,7}^{eff}$ (compare Fig. 5) we obtained effective activation energies for cluster sizes up to $i = 10$. The resulting solution of the rate equations is plotted in Fig. 6(a) as dashed line, which approaches at high temperatures the Boltzmann distribution of the 10-atom cluster shown as dotted dashed line. The effect of extending the range of mobile clusters is essentially to extend the temperature range of the base level toward higher temperatures. We note, however, that the used effective activation barriers for cluster sizes $i \geqslant 7$ is just a reasonable assumption with no physical basis. Other assumptions would influence our results differently. We additionally note that, as can be read from Fig. 6(a), T_c for the heptamer solution (heptamer is the largest mobile cluster) is given as the temperature at which this solution starts to deviate from the 10-atom cluster solution (10-atom cluster is the largest mobile cluster). Finally, in the calculations we assumed random deposition of the monomers on the two types of sites, yielding $n_x^h/n_x^f = 1$ at temperature below the onset of monomer diffusion. Assuming transient mobility one might argue as the alternative limit for the monomers to obey a Boltzmann distribution even beyond the onset of thermal mobility. This difference influences the results only for temperatures below the onset of dimer mobility. In the temperature ranges, in which the calculations are displayed in Figs. 6(a)–6(c), both assumptions yield identical results.

In the following we want to focus in the discussion on a comparison of the base levels for the three cases (I, II, and III) represented by Figs. 6(a)–6(c). For case I (high stacking-fault energy and low mobility), the base level of the stacking-fault probability is about 10^{-7} and stays within this range until T_c. For case II (low stacking-fault energy and low mobility), the stacking-fault probability in the base level stays around 0.1. It is not surprising that a lower ΔE_b leads to higher probability for stacking-fault formation. At a given temperature, due to identical mobilities, the numbers $i^\dagger$ for the two cases are identical. We obtain with Eq. (7) that $P^I/P^{II} \approx e^{-i^\dagger(\Delta E_b^I - \Delta E_b^{II})/k_B T}$, where the I and II denote the respective numbers for the two cases. Apparently, with $\Delta E_b^I > \Delta E_b^{II}$ the ratio P^I/P^{II} becomes much smaller than unity as seen also by comparison of Figs. 6(a) and 6(b). For case III

the stacking-fault probability in the base level is again low, around 10^{-8}. This appears surprising at first glance, because for case III the same low stacking-fault energy as in case II is used. The difference of seven orders of magnitude in stacking-fault probability is apparently only due to the increased cluster mobilities. With the help of Eq. (7) this can be understood as follows. For a given temperature, for the high-mobility case III, the largest mobile cluster is much larger than for the low-mobility case II (i.e., $i^{\dagger,\mathrm{III}} \gg i^{\dagger,\mathrm{II}}$). Thus we obtain $P^{\mathrm{III}}/P^{\mathrm{II}} \approx e^{-(i^{\dagger,\mathrm{III}}-i^{\dagger,\mathrm{II}})\Delta E_b/k_\mathrm{B}T}$, a number much smaller than unity, as is also apparent by comparison of Figs. 6(b) and 6(c). Comparing the effect of stacking-fault energy to the effect of cluster mobility, we find that a variation by a factor of about four in the associated energetic parameters gives a similar effect on the stacking-fault probabilities (6–7 orders-of-magnitude variation). Therefore the effect of cluster mobility is equally important for stacking-fault island formation as the effect of stacking-fault energy.

Comparison with measured data shows that the calculation results are in qualitative agreement with the experimental findings (see Table I). For the system Ag/Ag(111) stacking-fault formation is observed experimentally.[14,54] This system is close to the model case II, for which the rate equations also predict significant stacking-fault island formation. No stacking-fault formation is predicted for a system like Pt/Pt(111) similar to model case I, as verified experimentally.[55] We should remark that the system Ir/Ir(111) does not behave like the model case I due to the unlike behavior of the difference in binding energy per atom with the cluster size (see Fig. 3). For a system with high stacking-fault energy and high mobility both factors disfavor fault island formation. Therefore it is no surprise that for Al/Al(111) stacking faults were never observed.[55] Somewhat unclear is the situation for Cu/Cu(111). This system is close to our model case III, for which essentially no stacking-fault islands are predicted. On nominally flat Cu(111) with miscut angle below 0.1° indeed no stacking-fault islands were observed in an STM study,[17] whereas a thermal energy atom-scattering study[16] finds significant stacking-fault formation on a sample with a miscut angle of ~1°. Possibly for Cu/Cu(111) steps play a crucial role in stacking-fault formation, an effect which is not included in our model.

V. CONCLUSIONS

In conclusion, a rate-equation approach was shown to adequately predict the kinetics of stacking-fault island formation for unreconstructed fcc metal surfaces. Using the atomistic input data for the Ir/Ir(111) system excellent agreement between measurements and calculations for flux and temperature dependence of island densities and stacking-fault probabilities is obtained. The study of three model cases, covering the known parameter space of stacking-fault energy and cluster mobility for fcc(111) metals, shows that a low stacking-fault energy and a low cluster mobility are equally important factors favoring stacking-fault island formation.

*Corresponding author: polop@physik.rwth-aachen.de
†Present address: Interdisciplinary Nanoscience Center (iNANO), Center for Atomic Scale Materials Physics (CAMP) and Department of Physics and Astronomy, University of Aarhus, 8000 Aarhus, Denmark.

[1] V. Potin, B. Gil, S. Charar, P. Ruterana, and G. Nouet, Mater. Sci. Eng., B **82**, 114 (2001).
[2] E. Valchewa, T. Paskova, and B. Monemar, J. Phys.: Condens. Matter **14**, 13269 (2002).
[3] N. Wang, K. K. Fung, and I. K. Sou, Appl. Phys. Lett. **77**, 2846 (2000).
[4] S.-K. Huong, J.-H. Cheng, T. Hanada, E. Kurtz, M. Oku, and T. Yao, J. Vac. Sci. Technol. A **20**, 1948 (2002).
[5] O. Robach, H. Isérn, P. Steadman, K. F. Peters, C. Quirós, and S. Ferrer, Phys. Rev. B **68**, 214416 (2003).
[6] W. Auwärter, M. Muntwiler, J. Osterwalder, and T. Greber, Surf. Sci. Lett. **545**, L735 (2003).
[7] M. Pratzer and H. J. Elmers, Surf. Sci. **550**, 223 (2004).
[8] J. Wiebe, L. Sacharow, A. Wachowiak, G. Bihlmayer, S. Heinze, S. Blügel, M. Morgenstern, and R. Wiesendanger, Phys. Rev. B **70**, 035404 (2004).
[9] M. Zheng, J. Shen, C. V. Mohan, P. Ohresser, J. Barthel, and J. Kirschner, Appl. Phys. Lett. **74**, 425 (1999).
[10] O. Pietzsch, A. Kubetzka, M. Bode, and R. Wiesendanger, Phys. Rev. Lett. **92**, 057202 (2004).
[11] R. N. Thomas and M. H. Francombe, Surf. Sci. **25**, 357 (1971).
[12] H. Grube and J. Boland, Surf. Sci. **407**, 152 (1998).
[13] K. Meinel, M. Klaua, and H. Bethge, Phys. Status Solidi A **110**, 189 (1988).
[14] C. Ammer, T. Schaefer, and M. Klaua, Phys. Status Solidi A **146**, 205 (1994).
[15] S. A. de Vries, W. J. Huisman, P. Goedtkindt, M. J. Zwanenburg, S. L. Bennet, and E. Vlieg, Phys. Rev. Lett. **81**, 381 (1998).
[16] J. Camarero, J. de la Figuera, J. J. de Miguel, R. Miranda, J. Álvarez, and S. Ferrer, Surf. Sci. **459**, 191 (2000).
[17] M. Giesen and H. Ibach, Surf. Sci. **529**, 135 (2003).
[18] C. Busse, C. Polop, M. Müller, K. Albe, U. Linke, and T. Michely, Phys. Rev. Lett. **91**, 056103 (2003).
[19] C. Busse, S. Baud, G. Bihlmayer, C. Polop, T. Michely, and S. Blügel, Phys. Rev. B **68**, 201401 (2003).
[20] C. Busse and T. Michely, Surf. Sci. **552**, 281 (2004).
[21] G. Zinsmeister, Vacuum **16**, 529 (1966).
[22] J. A. Venables, Philos. Mag. **27**, 697 (1973).
[23] D. Kandel, Phys. Rev. Lett. **78**, 499 (1997).
[24] M. Kotrla, J. Krug, and P. Šmilauer, Phys. Rev. B **62**, 2889 (2000).
[25] J. A. Venables, and J. H. Harding, J. Cryst. Growth **211**, 27 (2000).
[26] S. Ovesson, Phys. Rev. Lett. **88**, 116102 (2002).
[27] J. A. Venables and H. Brune, Phys. Rev. B **66**, 195404 (2002).
[28] E. Vasco, C. Polop, and E. Rodríguez-Cañas, Phys. Rev. B **67**, 235412 (2003).

[29] E. Vasco, Phys. Rev. B **69**, 075412 (2004).
[30] S. C. Wang, U. Kürpick, and G. Ehrlich, Phys. Rev. Lett. **81**, 4923 (1998).
[31] S. C. Wang and G. Ehrlich, Surf. Sci. **239**, 301 (1990).
[32] C. Busse, Ph.D. thesis, RWTH Aachen (2003), available online at http://www.bth.rwth-aachen.de/job/disslist.pl
[33] H. Brune, Surf. Sci. Rep. **31**, 121 (1998).
[34] C. Busse, W. Langenkamp, C. Polop, A. Petersen, H. Hansen, U. Linke, P. J. Feibelman, and T. Michely, Surf. Sci. Lett. **539**, L560 (2003).
[35] S. C. Wang and G. Ehrlich, Phys. Rev. Lett. **68**, 1160 (1992).
[36] N. M. Rosengaard and H. L. Skriver, Phys. Rev. B **47**, 12865 (1993).
[37] S. Papadia, B. Piveteau, D. Spanjaard, and M. C. Desjonqueres, Phys. Rev. B **54**, 14720 (1996).
[38] A. Gross (private communication).
[39] For Ir clusters with $1 \leqslant i \leqslant 4$ the difference in free energy per atom $(\Delta F_i/i)$ is shown.
[40] A. Gölzhäuser and G. Ehrlich, Phys. Rev. Lett. **77**, 1334 (1996).
[41] J. Repp, G. Meyer, K. H. Rieder, and P. Hyldgaard, Phys. Rev. Lett. **91**, 206102 (2003).
[42] J. P. Hirth and J. Lothe, *Theory of Dislocations* (Krieger Publ., Melbourne, FL, 1992).
[43] L. E. Murr, Scr. Metall. **6**, 203 (1972).
[44] D. R. Lide, *CRC Handbook of Chemistry and Physics*, 78th ed. (CRC Press, Boca Raton, 1997/1998).
[45] L. E. Murr, Acta Metall. **21**, 791 (1973).
[46] M. Bott, M. Hohage, M. Morgenstern, T. Michely, and G. Comsa, Phys. Rev. Lett. **76**, 1304 (1996).
[47] K. Kyuno, A. Gölzhäuser, and G. Ehrlich, Surf. Sci. **397**, 191 (1998).
[48] G. Ayrault and G. Ehrlich, J. Chem. Phys. **60**(1), 281 (1974).
[49] T. Y. Fu, and T. T. Tsong, Surf. Sci. **454–456**, 571 (2000).
[50] H. Brune, K. Bromann, H. Röder, K. Kern, J. Jacobsen, P. Stoltze, K. Jacobsen, and J. Nørskov, Phys. Rep. **52**, R14380 (1995).
[51] C. Polop, H. Hansen, C. Busse, and T. Michely, Phys. Rev. B **67**, 193405 (2003).
[52] C. M. Chang, C. M. Wei, and S. P. Chen, Phys. Rev. Lett. **85**, 1044 (2000).
[53] K. Kyuno and G. Ehrlich, Surf. Sci. **437**, 29 (1999).
[54] P.-W. Chung, C. Ghosh, M. Li, J. W. Evans, and P. A. Thiel (unpublished).
[55] T. Michely (unpublished).